Electronic structures of FeB, Fe_2B, and Fe_3B compounds studied using first-principles spin-polarized calculations

W. Y. Ching and Yong-Nian Xu
Department of Physics, University of Missouri–Kansas City, Kansas City, Missouri 64110

B. N. Harmon, Jun Ye, and T. C. Leung
Ames Laboratory and Department of Physics, Iowa State University, Ames, Iowa 50011
(Received 23 April 1990)

The band structures of the ferromagnetic compounds FeB, Fe_2B, and Fe_3B were calculated using a spin-polarized version of the first-principles self-consistent orthogonalized linear-combination-of-atomic-orbitals method. Results on the band structure, density of states (DOS), and site-, orbital-, and spin-decomposed partial DOS are presented. Mulliken population analysis indicates B to be an electron accepter in these compounds due to the low-lying levels of the B $2s$ and B $2p$ states relative to the Fermi level. It is also shown that the moment on B is slightly polarized opposite to the Fe moments. The magnetic structure and bonding in these three compounds are further revealed by the presentation of contour maps for the charge density and the spin density. Our calculation shows an average spin magnetic moment of 1.26, 1.95, and $1.94\mu_B$ per Fe site and -0.10, -0.23, and $-0.29\mu_B$ per B site in FeB, Fe_2B, and Fe_3B, respectively. The results are in reasonable agreement with photoemission and neutron-scattering measurements. The nature of the Fe—B bond is discussed in connection with the electronic structure of $Nd_2Fe_{14}B$ intermetallic compounds and that of the $Fe_{1-x}B_x$ metallic glasses.

I. INTRODUCTION

The intermetallic Fe-B compounds have been subjected to intense experimental and theoretical investigations.[1–4] This is not only because these materials have vast applications due to their special mechanical, electrochemical, and magnetic properties, but also because the physics and chemistry of the Fe-B system are highly interesting and remain controversial.[3] The Fe-B compounds are hard and brittle ferromagnetic metals. The nature of electronic bonding in Fe-B compounds is the subject of several theoretical models.[1–3] In the past, Fe_2B and FeB crystals have been studied in considerable detail, while Fe_3B was mostly discussed in the context of a-$Fe_{1-x}B_x$ metallic glasses.[5,6]

There are two previous theoretical calculations of the electronic structures of FeB and Fe_2B.[3,4] The most recent one was by Li and Wang for FeB and Fe_2B crystals using the self-consistent linear augmented-plane-wave (LAPW) method without spin polarization.[4] Since study of the magnetic properties of the Fe-B compounds is our prime motivation, we carried out spin-polarized calculations for these compounds. In this paper, we present the results of self-consistent spin-polarized calculations for FeB, Fe_2B, and in addition, the Fe_3B compound, using the first-principles orthogonalized linear-combinations-of-atomic-orbitals method (OLCAO). Together with calculated results on the crystalline bcc Fe, our study gives a complete picture of the electronic structure and binding in Fe-B compounds with increasing B concentration. Such results should be of value in understanding the electronic structure and magnetic properties of $Fe_{1-x}B_x$ glasses. Furthermore, our results also provide additional insight into the electronic structure of $Nd_2Fe_{14}B$, the newly discovered hard magnetic compound that has gained much attention in recent years, but for which there is yet little theoretical understanding.

The paper is organized as follows. We will briefly describe the crystal structures of the Fe-B compounds in Sec. II, focusing mainly on the local short-range order. The method used for the spin-polarized calculation is described in Sec. III, and the results on the three crystals are presented in Sec. IV. These results are further discussed and a comparison is made with experimental data in Sec. V. The last section is devoted to some concluding remarks.

II. CRYSTAL STRUCTURES

FeB crystallizes in an orthorhombic structure with 4 formula units (f.u.) per cell[7] and the space group is *Pnma* as given in Table I. The Fe-B nearest-neighbor (NN) distances range from 2.145 to 2.210 Å. The B-B distances alternate with 1.802, 2.953, and 2.949 Å in forming a zigzag chain. The Fe-Fe distances range from 2.627 to 2.953 Å, which is considerably larger than the 2.482 Å in the bcc Fe.

Fe_2B has a body-centered tetragonal structure with a space group of $I4/mcm$ and 2 f.u. per cell.[8] The structure can be viewed as consisting of alternate layers of Fe and B atoms. The Fe atoms may be considered as forming a distorted tetrahedron with the Fe-Fe distances of 2.414, 2.440, 2.692, and 2.725 Å. Thus two of the Fe-Fe NN distances in Fe_2B are shorter and the other two

longer than that of bcc Fe. There is only one Fe-B distance of 2.180 Å and one B-B distance of 2.124 Å.

Two phases of Fe_3B have been identified, the body-centered tetragonal (bct) phase and the orthorhombic phase. The orthorhombic Fe_3B is believed to be less stable than the tetragonal phase. Both phases can be obtained by quenching and annealing from the Fe-B glasses.[5] In this study, we only consider the orthorhombic phase that is isostructural with the Fe_3C (cementile) with a space group of *Pbnm*.[9] The unit cell contains 4 f.u. There are two different Fe sites, the Fe (4*c*) and the Fe (8*d*) and one B site (4*c*) for a total of 16 atoms in the cell. The Fe-B NN distances range from a low of 2.001 Å to a high of 2.811 Å. The B-B distances are much larger, ranging from 3.142 to 4.450 Å. The Fe-Fe distances are intermediate between those in FeB and Fe_2B, ranging from 2.512 to 2.761 Å, all are larger than the crystalline Fe-Fe distance. Thus the short-range order in FeB, Fe_2B, and Fe_3B does not necessarily correlate with the B concentration, but depends on the actual crystal symmetry of each compound. The short-range order in the bct Fe_3B may already resemble that of a-$Fe_{75}B_{25}$ glass in which the metalloid-metalloid NN configuration is not expected.

The structural information for the three Fe-B crystals including the lattice constants and the NN distances are summarized in Table I.

III. METHOD OF CALCULATION

The OLCAO method in the local-density approximation has been widely used to study the electronic structure of a variety of condensed-matter systems including semiconductors,[10,11] insulators,[12] metals,[13] and intermetallic compounds,[14] oxide superconductors,[15,16] and even amorphous systems.[17] The use of an atomic basis to expand the Bloch functions results in a very economic basis set and as a result, the method can be applied to crystals with large unit cells and complex structures. In recent years, the method has been used to study the ground-state properties via total-energy calculations.[10] Even more recently, the method has been extended to include spin polarization and has been applied to study the magnetic properties of high-T_c superconductors.[16] Very recently, relativistic corrections have also been added to this method.[18] However, in the present study for Fe-B compounds, we have totally ignored relativistic effects.

The OLCAO method has also been used to study the electronic and magnetic properties of $Nd_2Fe_{14}B$ and related permanent magnets with considerable success.[14] Although, the calculation was spin-polarized, the crystal potential was not self-consistently derived because the unit cell of $Nd_2Fe_{14}B$ consists of 68 atoms.[19] Instead, optimum atomiclike potentials for the majority- and minority-spin states were constructed using atomic spin splitting information and the crystalline band structure as a guideline. The role played by the B atom and the nature of the Fe—B bonding in $Nd_2Fe_{14}B$ was less conclusive because of the non-self-consistent nature of the calculation.[14]

In the present calculation for the Fe-B compounds, we expand the Bloch function in terms of 1*s*, 2*s*, 3*s*, 4*s*, 2*p*,

TABLE I. Crystal structure information of FeB, Fe_2B, and Fe_3B. The numbers in parentheses represent the number of bonds.

	FeB	Fe_2B	Fe_3B	Fe
Crystal structure	Orthorhombic	bct	Orthorhombic	bcc
Lattice const (Å)	$a=5.5076$	$a=5.110$	$a=4.4500$	$a=2.8663$
	$b=2.9528$		$b=5.4052$	
	$c=4.0625$	$c=4.249$	$c=6.6685$	
Z (mol/cell)	4	2	4	1
Space group	*Pnma*	*I4/mcm*	*Pbnm* (V_h^{16})	
NN Dist. (Å)	2.1455(2)	2.1799(8)	2.0060(2)	
	2.1710(2)		2.1038(2)	
Fe-B	2.1719(1)		2.3630(2)	
	2.2095(1)			
	2.1743(1)		2.0150(1)	
			2.0721(1)	
			2.8110(1)	
B-B	1.8019(2)	2.1245(2)	3.1417	
	2.9494(2)		3.6715	
	2.9527(1)		3.9261	
Fe-Fe	2.6268(4)	2.4136(1)	2.5116(2)	2.4823(8)
	2.6725(2)	2.4397(2)	2.6048(2)	
	2.9351(2)	2.6921(4)	2.6466(4)	
	2.9527(1)	2.7251(4)	2.7610(2)	

$3p$, $4p$, and $3d$ atomic orbitals of Fe and $1s, 2s$, and $2p$ states of B. Each of the atomic radial functions are expanded in terms of up to 15 Gaussian types of orbitals, with exponentials ranging from 50 000 to 0.15. The crystal potential is constructed according to a local spin-density formalism using the von Barth–Hedin[20] form of the exchange and correlation potential as modified by Moruzzi *et al.*[21] Both the spin-dependent potential and the spin- and charge-density functions are expressed as a sum of atom-centered Gaussian functionals. In each of the self-consistent iterations, the coefficients of the expansion are obtained by linearly fitting the spin- and charge-density functions to the data set of the actual spin and charge density calculated from the Bloch functions at a large number of real-space points. The accuracy of the calculation depends critically on the quality of the fit. In the present study, we have achieved an accuracy of limiting the unconstrained fitting error to less than 0.000 86, 0.000 47, and 0.001 66 electron per valence electron for FeB, Fe_2B, and Fe_3B, respectively. This level of fitting accuracy is more than adequate for the electronic structure studies. Ten special **k** points are used for the self-consistency, while the final calculation involved 144, 125, and 144 **k** points in the irreducible part of the Brillouin zone for FeB, Fe_2B, and Fe_3B, respectively. For metallic systems such as the Fe-B compounds, a sufficient number of **k** points must be used for an accurate determination of the Fermi energy (E_F). In the spin-polarized calculation, we found it necessary to give an initial polarization to the Fe moment for the first few iterations to ensure a stable iterative process. The convergence to self-consistency in the spin-polarized calculation is much slower than the non-spin-polarized calculation for the same system. No special techniques are employed to speed up the convergence, and it takes about 100 iterations to get full convergence for each compound studied. This slow convergence is related to the fact that the final B moment is negatively polarized and the system is slow in readjusting its spin-density distribution.

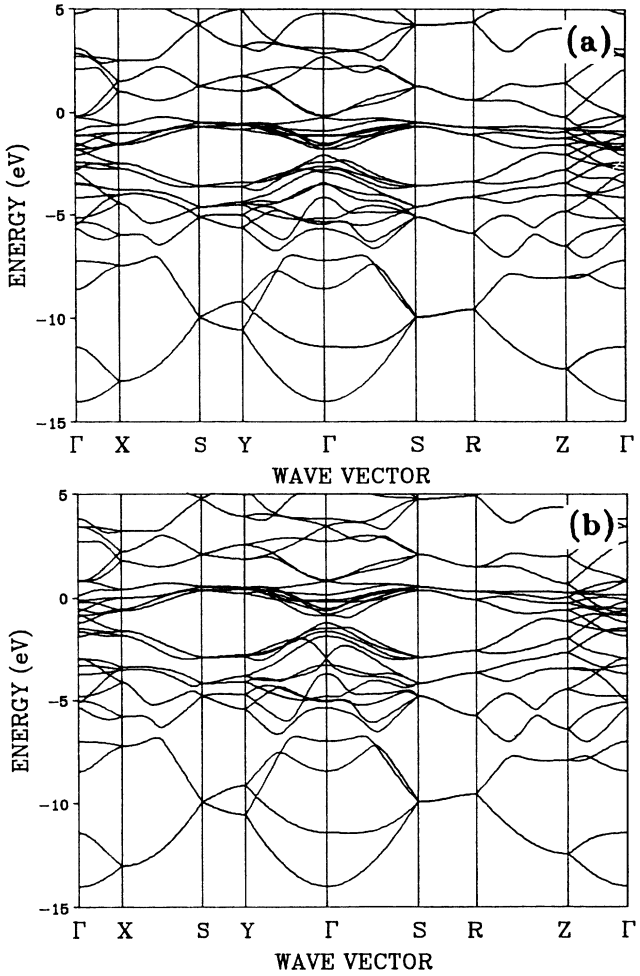

FIG. 1. Band structure of FeB. (a) majority-spin band; (b) minority-spin band.

IV. RESULTS

A. FeB

The calculated majority (spin-up) and the minority (spin-down) bands for FeB along the symmetry directions of the orthorhombic cell are shown in Fig. 1. At about -7.0 eV, the band structures show a small gap (indirect gap). Below this gap, the states are predominantly derived from the B $2s$ states. The total density of states (DOS) and the orbital-resolved partial DOS (PDOS) for both spins added together are shown in Fig. 2. The DOS curve is rich in structure. The Fermi level lies at the top of a small peak in the valley of two large peaks originating from the exchange splitting. The peak at the E_F comes from the minority-spin band. The major features of Fig. 2 can be summarized as follows: (1) The majority of the occupied states are from the Fe $3d$ states extending down to -10 eV. (2) The Fe $4s$ and $4p$ states are delocalized and extend down to -14 eV. (3) The B $2s$ states extend from -14 to -3 eV, with a major peak at -12.1 eV. The occupied portion of the B $2p$ states extend from -14 eV to E_F, with a major peak near -4 eV, which drops very sharply at -3 eV. From this PDOS diagram, the binding picture in the Fe-B compound clearly emerges. First, the B states are mostly confined to the -14 to -3 eV region, well below the Fermi level, the do not seem to be strongly interacting with the relatively localized Fe $3d$ states. The substantial portion of B $2p$ states above E_F must come from the antibonding states of Fe and B. Even with a high B concentration of 50% in the FeB compound, the Fe $3d$ PDOS is still quite similar to that of the pure bcc Fe.[21] On the other hand, the delocalized Fe $4s$ and $4p$ orbitals hybridize with the B states rather effectively. Since hybridized B states are considerably below the E_F, B must be an electron acceptor with charges transferred from the nearby Fe atoms. It is interesting to point out that the free-atom calculation[22] gave the orbital energy levels of B $2s$ and $2p$ to be $-0.494\,68$ and $-0.309\,87$ a.u., considerably higher than the Fe $3d$ level of $-0.647\,10$ a.u.

The charge-density $[\rho_\uparrow(r)+\rho\downarrow(r)]$ map and the spin-density map $[\rho_\uparrow(r)-\rho\downarrow(r)]$ in a plane containing two Fe atoms and a B atom in FeB are shown in Fig. 3. The

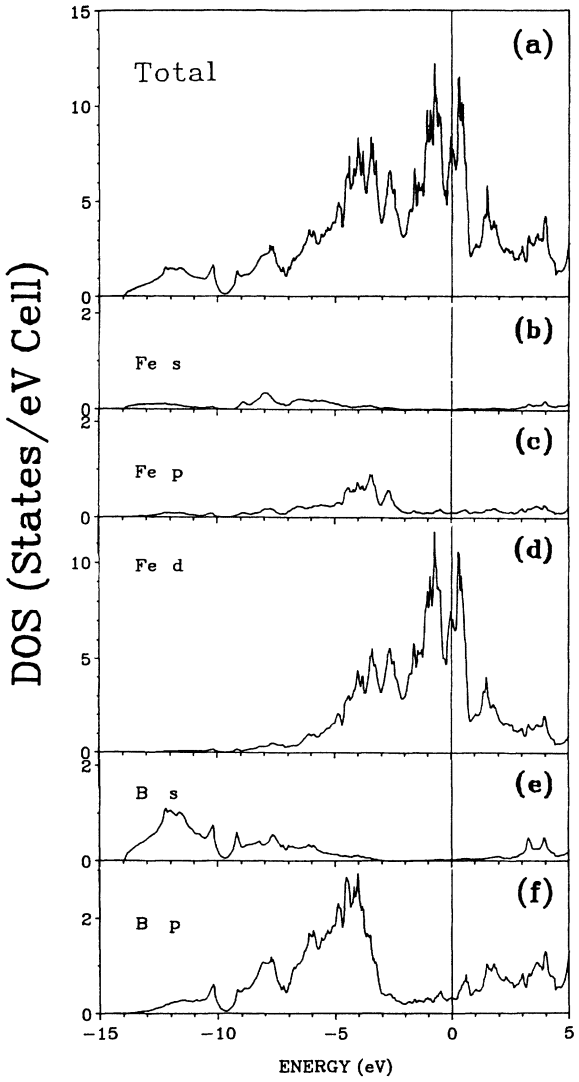

FIG. 2. Density of states of FeB. (a) Total; (b) Fe 4*s*; (c) Fe 4*p*; (d) Fe 3*d*; (e) B 2*s*; (f) B 2*p*.

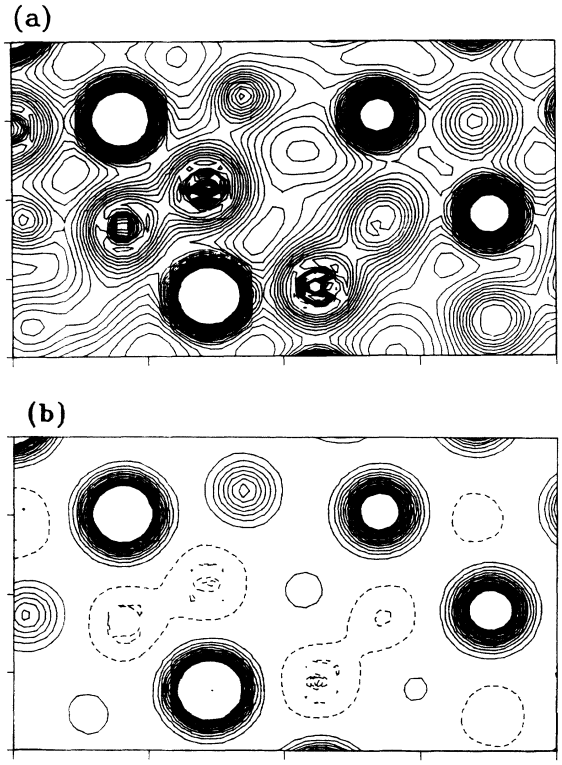

FIG. 3. (a) Charge density in FeB in a plane. The contours are from 0.01 to 0.25 a.u.$^{-3}$ in units of 0.005 a.u.$^{-3}$; (b) spin density in FeB in the same plane. The contours are from 0.002 to 0.04 a.u.$^{-3}$ in units of 0.001 a.u.$^{-3}$. Dashed lines indicate negative values.

charge-density map shows there is some covalent binding between the Fe and B atoms as well as the B-B atoms. The present result of charge distribution is very similar to that of Ref. 4 using the LAPW method. The spin-density map in Fig. 3 shows the B atoms are negatively polarized in the direction opposite to the Fe moments. This is consistent with the neutron-scattering measurements.[1,2]

B. Fe_2B

The calculated majority- and minority-spin bands for Fe_2B are shown in Fig. 4. The small gap near -7.0 eV in FeB is no longer present in Fe_2B. This is more likely due to the different crystal symmetries rather than the difference in the B concentration. The bottom of the bands that consist mostly of B 2*s* orbitals is at -12.5 eV, higher than the -14 eV of the FeB bands. This reduction in the overall bandwidth is attributed to the decreased B-B interaction as the PDOS of B is reduced. The calculated total DOS and the orbital resolved PDOS are shown in Fig. 5. Other than the reduction in the bandwidth and the contribution from the B atoms, the overall features of the DOS spectra are quite similar to that of the FeB. The structures in the Fe 3*d* PDOS are slightly different, reflecting the structural differences in the two crystals, such as the presence of shorter Fe-Fe NN distances in Fe_2B. Such a difference can be detected experimentally, which will be discussed in more detail in Sec. V. Like FeB, the Fermi level lies at the top of a sharp peak originating from the minority-spin band.

The charge density and the spin density of Fe_2B in the (120) plane are shown in Fig. 6. There is still some degree of covalent bonding between the B-B atoms at a distance of 2.12 Å, which is larger than that in FeB. The later has a shorter B—B bond of 1.80 Å. The B atoms in Fe_2B also have a negative spin density with a nonspherical distribution as shown in Fig. 6(b). The negative polarization on the B atom is significantly larger than in FeB. This is probably because when the B concentration is reduced, there is an increased influence from the surrounding Fe atoms on each of the B atom.

C. Fe_3B

The calculated majority- and minority-spin bands in bct Fe_3B are shown in Fig. 7. The much more dense

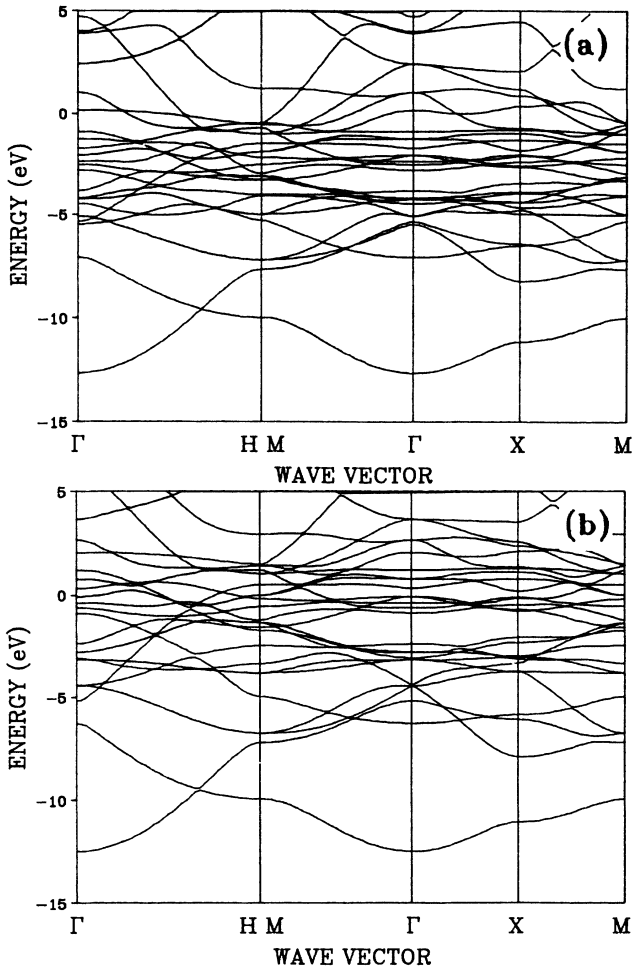

FIG. 4. Band structure of Fe_2B. (a) majority-spin band; (b) minority-spin band.

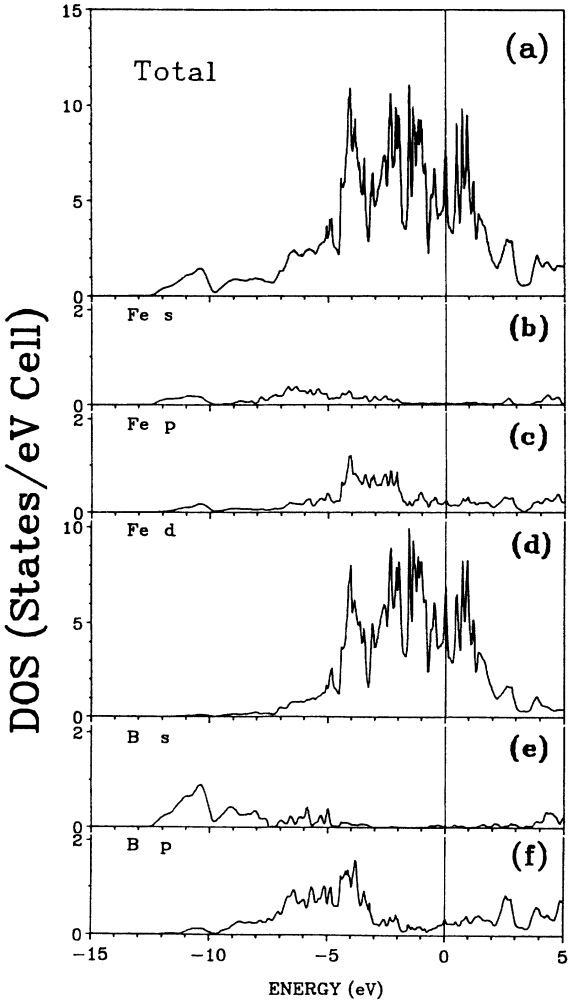

FIG. 5. Density of states of Fe_2B. (a) Total; (b) Fe 4*s*; (c) Fe 4*p*; (d) Fe 3*d*; (e) B 2*s*; (f) B 2*p*.

bands reflect the complexity of the primitive cell containing 16 atoms. Like FeB, there is a gap deep in the bands at about -7.0 eV. Unlike FeB, this gap of about 0.8 eV is direct at Γ. The bottom of the bands is -11.1 eV below the Fermi level, which is higher than for Fe_2B. This is again due to the much weaker B-B and Fe-B interactions as reflected by the NN interatomic distances shown in Table I. The calculated DOS and PDOS spectra for Fe_3B are shown in Fig. 8. Comparing with the same spectra for FeB and Fe_2B, it is clear that the bandwidth is greatly reduced and its features are shifted towards the Fermi level. Because of the large number of atoms in the unit cell of Fe_3B, the DOS resembles that of a-$Fe_{75}B_{25}$, which will be discussed further in Sec. V. The Fermi level does not coincide with a peak in the DOS as in the cases of FeB and Fe_2B. Thus, in spite of the increased Fe concentration, the DOS at E_F per Fe atom in Fe_3B is actually less than that of FeB and Fe_2B.

The charge-density map and the spin-density map in F_3B in a plane containing two Fe atoms and a B atom are shown in Fig. 9. Because of the decreased B concentra-

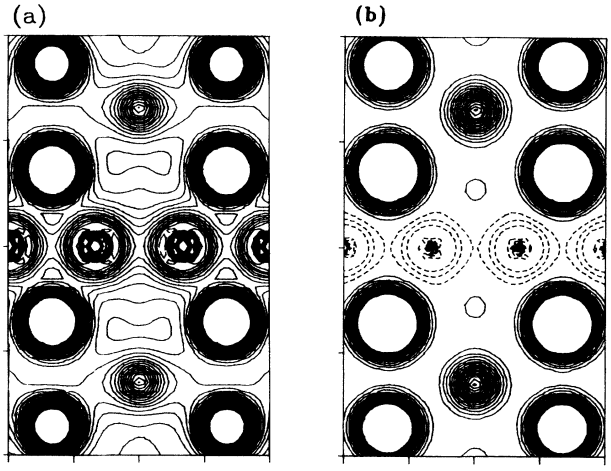

FIG. 6. (a) Charge density in Fe_2B in the [210] plane. The contours are from 0.01 to 0.25 a.u.$^{-3}$ in units of 0.005 a.u.$^{-3}$; (b) spin density in Fe_2B in the same plane. The contours are from 0.002 to 0.04 a.u.$^{-3}$ in units of 0.001 a.u.$^{-3}$. Dashed lines indicate negative values.

tion, the Fe—Fe metallic bond is similar to that in bcc Fe, while the Fe—B covalent bond is similar to those of FeB and Fe_2B. The spin-density map shows that B is even more negatively polarized with a distribution that is highly nonspherical. The covalent nature of the Fe—B bond and the fact that charges are transferred from the Fe to B atoms in the *bond region* are quite evident in Fig. 10, in which we plot the charge and spin density along the Fe—B bond. Also shown is the charge density of the neutral Fe and B atoms placed at the same site.

The effective charges Q^* and their orbital and spin components calculated according to the Mulliken scheme for each atom in all three crystals are listed in Table II. Also listed are the spin magnetic moments M_s on the Fe and B sites and the values of the DOS at the Fermi level. We have obtained the Fe M_s values at 1.26 and $1.95\mu_B$ for FeB and Fe_2B, respectively, which compare favorably with the experimental values of 0.9 and $1.6\mu_B$, respectively.[1,2] For Fe_3B, we obtained the Fe M_s values of 1.91 and $2.01\mu_B$ for the two different Fe sites. This difference in M_s Fe moments between two different Fe sites indi-

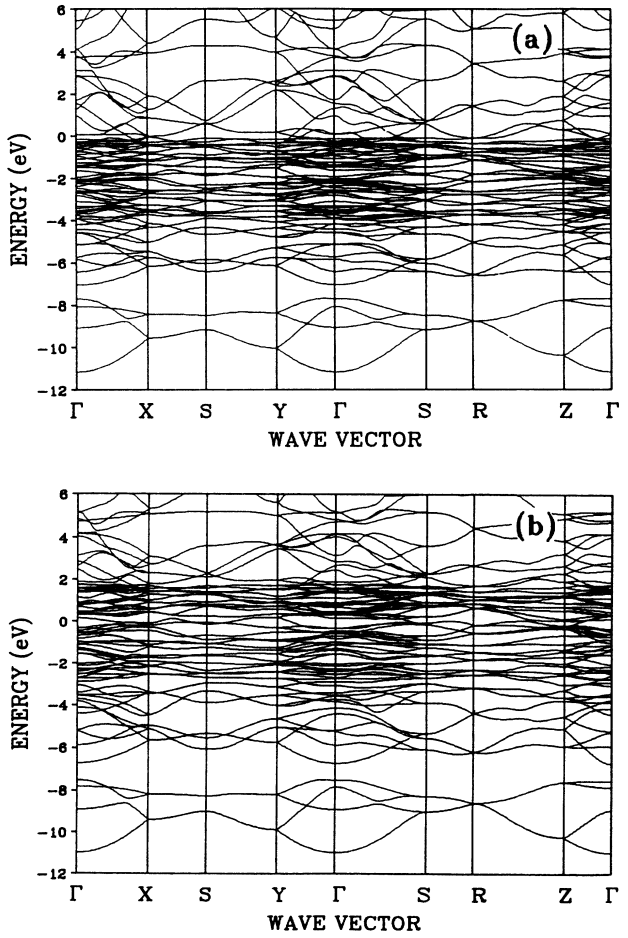

FIG. 7. Band structure of Fe_3B. (a) majority-spin band; (b) minority-spin band.

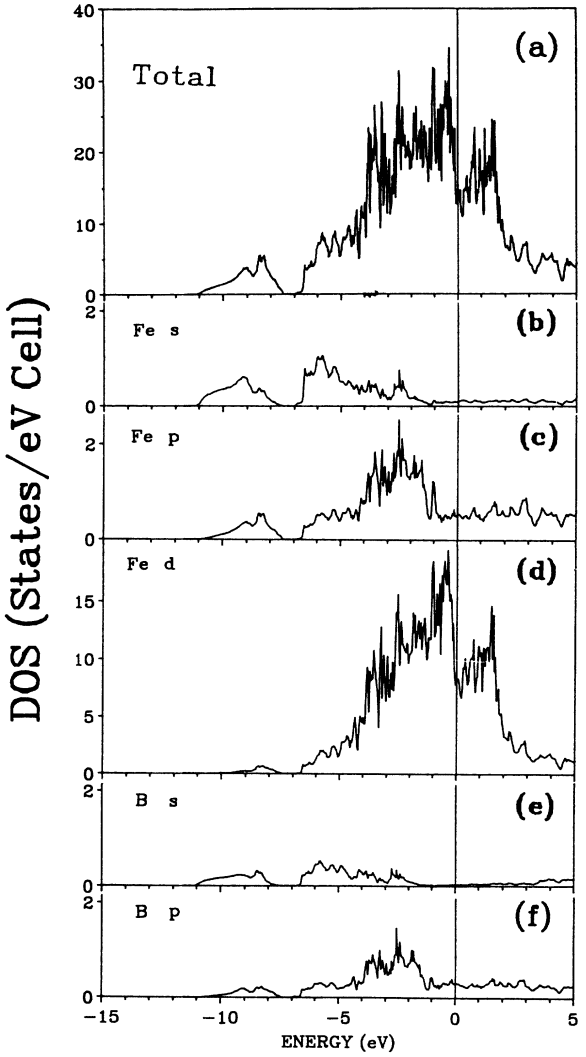

FIG. 8. Density of states of Fe_3B. (a) total; (b) Fe 4*s*; (c) Fe 4*p*; (d) Fe 3*d*; (e) B 2*s*; (f) B 2*p*.

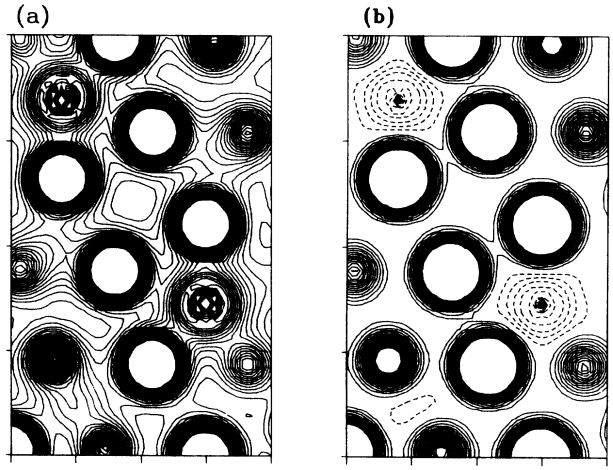

FIG. 9. (a) Charge density in Fe_3B in a plane containing the Fe—B—Fe NN bonding configuration. The contours are from 0.01 to 0.25 a.u.$^{-3}$ in units of 0.005 a.u.$^{-3}$; (b) spin density in Fe_2B in the same plane. The contours are from 0.002 to 0.04 a.u.$^{-3}$ in units of 0.001 a.u.$^{-3}$. Dashed lines indicate negative values.

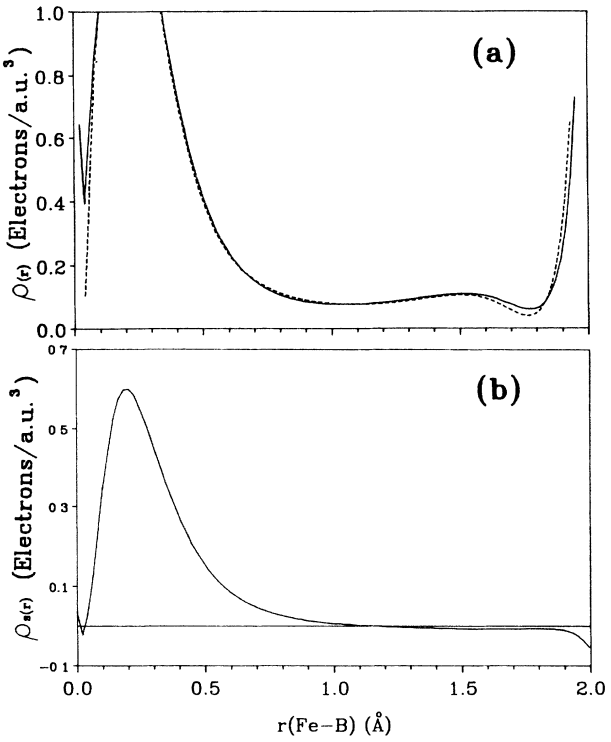

FIG. 10. (a) Valence charge density and (b) spin density along a Fe—B bond in Fe_3B. The dashed line is the same quantity from the superposition of neutral atoms.

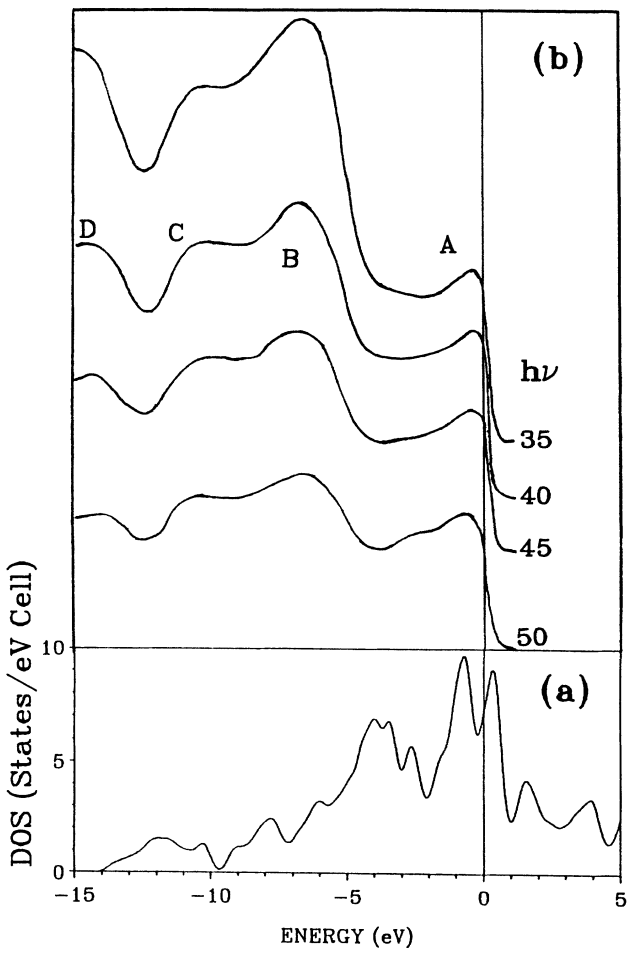

FIG. 11. Comparison of (a) broadened theoretical DOS curve with (b) the experimental photoemission data from Ref. 3 for FeB.

cates that the Fe moments are sensitive to the local short-range order in the crystal. No experimental values for M_s in crystalline Fe_3B are available for comparison. The M_s value per Fe in a-$Fe_{75}B_{25}$ is about $1.9\mu_B$ (Ref. 24). These values are certainly consistent with the bcc Fe moment of $2.15\mu_B$. The total average effective charge per Fe atom in FeB, Fe_2B, and Fe_3B are 7.46, 7.73, and 7.82 ($8d$ site) and 7.95 ($4c$ site), respectively. The corresponding Q^* for a B atom are 3.45, 3.55, and 3.57 electrons. Thus generally speaking, each B atom gains about half an electron due to the charge transfer from the Fe atom in all three Fe-B crystals.

The B atoms are oppositely polarized in all the three crystals as indicated by the spin-density maps. The effective charge calculation gives the B moments of -0.10, -0.23, and $-0.29\mu_B$ for FeB, Fe_2B, and Fe_3B, respectively. Hence, the negatively polarized M_s for B correlates with the B concentration. We will discuss this point again in Sec. V in connection with the magnetic properties of $Fe_{1-x}B_x$ glasses.

V. DISCUSSION

In this section we will compare our calculated results with the available experimental measurements. Detailed photoemission measurements have been carried out with FeB, Fe_2B, and Fe_3B crystals.[3,23] In Figs. 11–13, we display the broadened theoretical total DOS and compare it with the experimental energy distribution curves in the three crystals. Of the three crystals, the best agreement is actually obtained for Fe_3B. In spite of the low-energy resolution in the photoemission spectra for FeB and Fe_2B,[3] it appears that all the major structures (labeled A, B, C, D, etc.) in the experimental curves have been reproduced by the calculation, although the positions of the peaks are not always exact. It is particularly puzzling that the peak D in the experimental curve for FeB is considerably off from the theoretical curve. It is not clear if this is due to some unexplained satellite peak or some sample contamination. We are fairly confident that this peak should not be the B $2s$ peak since the agreement between theory and experiment in the B $2s$ peak in Fe_2B and Fe_3B is quite good. Nevertheless, the agreement in peak positions is much better than that of Ref. 4, calculated using the self-consistent LAPW method. This may indicate the importance of including spin polarization into the calculation that modifies peak positions in the total DOS spectra.

The magnetic properties of FeB and Fe_2B have been probed by neutron-scattering experiments by Perkins and Brown[2] and Brown and Cox.[1] They concluded that B is

TABLE II. Calculated effective charges Q^*, spin magnetic moments M_s, and DOS at the Fermi level (in units of states/eV spin cell) for FeB, Fe_2B, Fe_3B, and Fe crystals.

	FeB	Fe_2B	Fe_3B		Fe
		Fe $Q^*_\uparrow$ (electron)			
			Fe (8*d*)	Fe (4*c*)	
s	0.148	0.208	0.226	0.234	0.301
p	0.316	0.374	0.387	0.391	0.389
d	3.984	4.260	4.245	4.359	4.446
Total	4.358	4.842	4.861	4.984	5.136
		$Q^*_\downarrow$ (electron)			
s	0.140	0.208	0.228	0.234	0.290
p	0.313	0.413	0.432	0.432	0.354
d	2.648	2.271	2.294	2.242	2.182
Total	3.102	2.896	2.954	2.966	2.825
$Q^*=Q^*_\uparrow+Q^*_\downarrow$	7.460	7.734	7.815	7.950	7.961
$M_s=Q^*_\uparrow-Q^*_\downarrow$	1.256	1.951	1.909	2.018	2.15*
M_s (Expt.) μ_B	0.9 (Ref. 2)	1.6 (Ref. 1)	1.9 (Ref. 17)		2.15
		B $Q^*_\uparrow$ (electron)			
s	0.512	0.546	0.553		
p	1.205	1.114	1.101		
Total	1.717	1.660	1.655		
		$Q^*_\downarrow$ (electron)			
s	0.533	0.597	0.600		
p	1.287	1.292	1.313		
Total	1.820	1.889	1.913		
$Q^*=Q^*_\uparrow+Q^*_\downarrow$	3.542	3.549	3.566		
$M_s=Q^*_\uparrow-Q^*_\downarrow$	−0.104	−0.229	−0.263		
$N(E_F)_\uparrow$	0.84	1.58	5.65		0.921
$N(E_F)^\downarrow$	6.70	5.875	7.65		0.294
$N(E_F)$ (total)	7.54	7.455	13.30		1.215

negatively polarized, in agreement with the present calculation, but did not give a quantitative value for the moment on a B atom. They had also established the measured magnetic moment per Fe atom to be $0.9\mu_B$ in FeB and $1.6\mu_B$ in Fe_2B, which are to be compared with our calculated values of $1.25\mu_B$ and $1.95\mu_B$ for the two crystals. For Fe_3B there is no data on crystalline samples, but magnetic measurements[24] on a-$Fe_{80}B_{20}$ films gave a value for the average Fe moment of about $1.90\mu_B$, which is to be compared to our calculated average value of $1.94\mu_B$ in the Fe_3B. The change in the Fe moment as a function of B concentration is more clearly demonstrated in Fig. 14, which shows the spin-projected PDOS for bcc Fe, FeB, Fe_2B, and Fe_3B. The reduction in the Fe moment as the B concentration is increased is due to the reduction in the exchange splitting. As the B concentration is increased, there is more admixture of B orbitals in the hybridized wave function, which causes a reduction in the exchange splitting. In Fig. 14 it is more clearly demonstrated that the prominent Fe 3*d* peak in the minority-spin band moves progressively towards the Fermi level as the B concentration is increased. Nevertheless, with 50% B concentration in FeB, the system is still ferromagnetic. The effective charge presented in Table II shows that the *s* and *p* electrons in Fe are almost the same for the spin-up and spin-down bands, so it is the *d* electrons in the Fe that are responsible for the ferromagnetism in Fe-B compounds. The role of the B atoms is in the hybridization of the wave function, which results in the lowering of the exchange splitting, rather than simple dilution; since the number of Fe-Fe NN pairs and the corresponding Fe-Fe distances in FeB and Fe_3B are not significantly different.

There have been many experimental and theoretical studies[24–32] in a-$Fe_{1-x}B_x$ glasses, which has a eutectic ratio around $x=0.20$. Early DOS calculations[27] on large cluster models of a-$Fe_{1-x}B_x$ glass show all of the B states are above E_F, which is clearly incorrect in light of the present self-consistent spin-polarized calculations. The more controversial issue in the glass system is whether the dependence of the average Fe moment on the B concentration is linear or nonlinear.[25] Assuming the Fe moments in amorphous and crystalline FeB compounds are

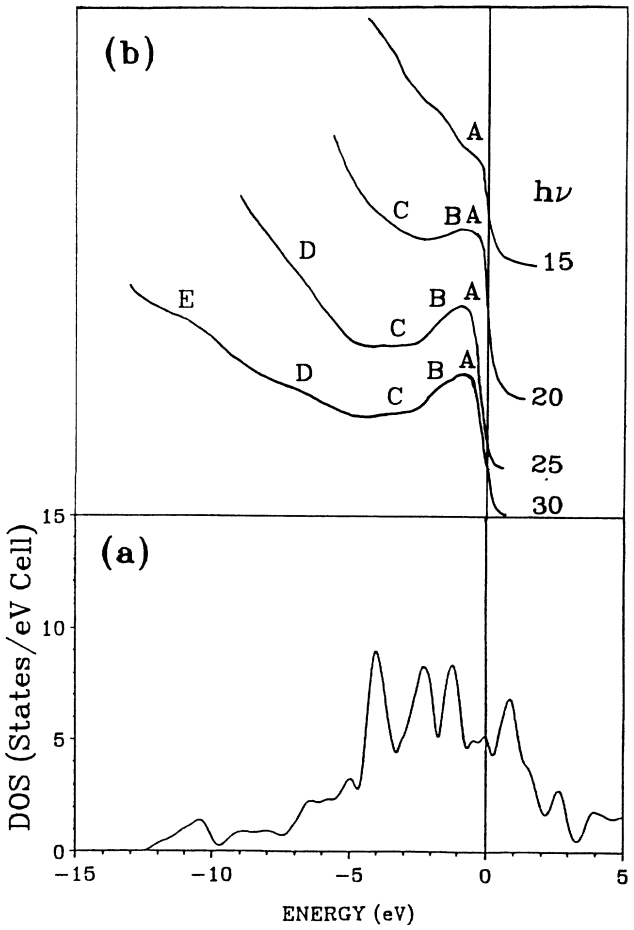

FIG. 12. Comparison of (a) broadened theoretical DOS curve with (b) the experimental photoemission data from Ref. 3 for Fe_2B.

similar for a similar type of local short-range order, our calculation seems to suggest that the dependence is probably nonlinear. This is illustrated in Fig. 15, in which we plot our calculated M_s values for the three crystals together with experimental data for a-$Fe_{1-x}B_x$. Although

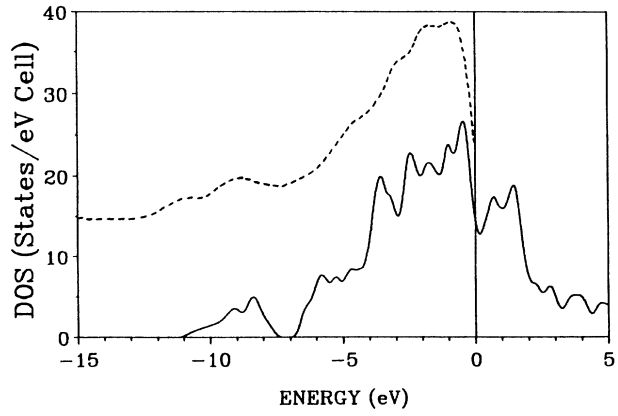

FIG. 13. Comparison of broadened theoretical total DOS curve of Fe_3B (solid line), with the experimental photoemission data from Ref. 16 (dashed line).

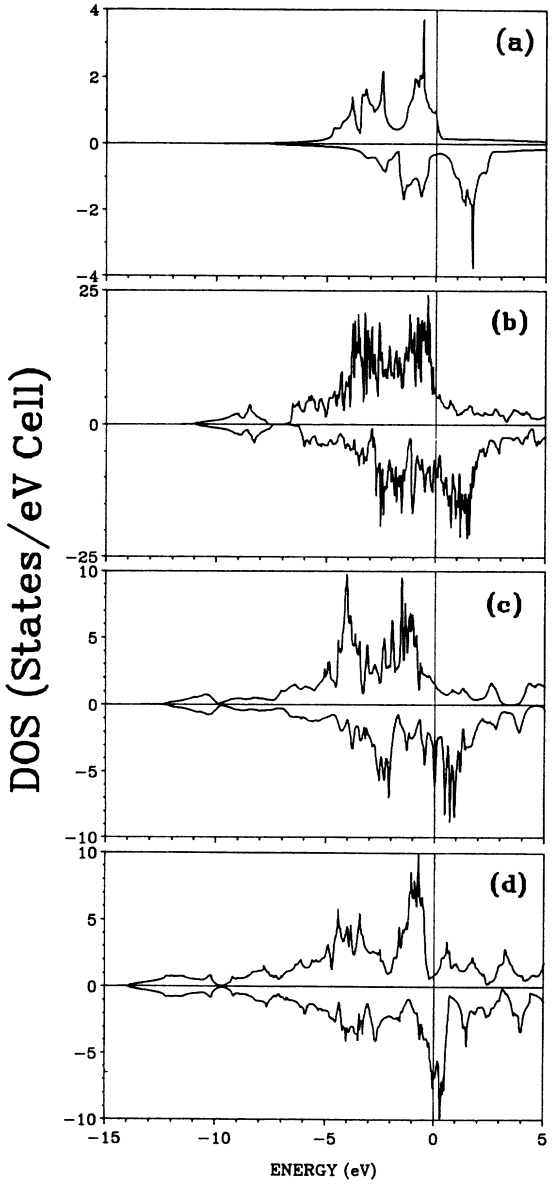

FIG. 14. Spin projected DOS for (a) fcc Fe; (b) Fe_3B; (c) Fe_2B; (d) FeB above 0 for the majority-spin bands and below 0 for the minority-spin band.

the M_s values for the crystals are slightly above the experimental data for amorphous films, the general nonlinear dependence on the B concentration is quite obvious. However, to have a more firm conclusion, realistic spin-polarized calculations must be performed on models of different B concentrations. The OLCAO method has been very successful in the study of electronic and transport properties of metallic glasses using large model calculations.[17] Calculation on magnetic glasses such as a-$Fe_{1-x}B_x$ should be a natural extension.

The rare-earth Fe-B compounds have attracted a great deal of research effort in recent years because of their superior permanent magnetic properties. It has long been

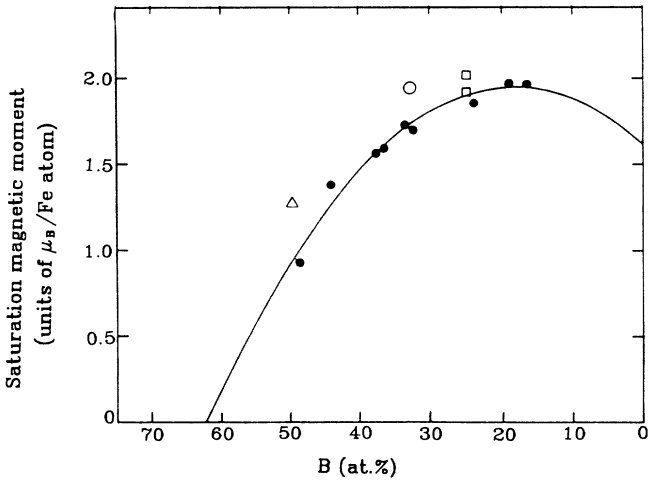

FIG. 15. Average magnetic moment per Fe in amorphous Fe-B films as shown in Ref. 18 and the result of the present calculation: △, FeB; ○, Fe_2B; □, Fe_3B.

recognized that B plays a crucial role in stabilizing the crystal structure of $Nd_2Fe_{14}B$ and related compounds.[19] We have studied the electronic and the magnetic properties of this crystal using the OLCAO method.[14] The main conclusion was that Fe and B form multiatom covalent bonds and that the spin density shows a network-like structure extending along the crystalline z direction, which may be related to its superior permanent magnetic properties. The calculated spin-magnetic moments for different Fe sites range from a low of $1.99\mu_B$ (e site) to a high of $3.40\mu_B$ ($j2$ site) and are in good agreement with neutron-scattering data. However, that calculation was not self-consistent because of the complexity of the crystal structure. Since the NN Fe-Fe and Fe-B distances in $Nd_2Fe_{14}B$ are comparable to those of the Fe-B compounds listed in Table I, we expect the bonding pattern and the spin-polarization between the Fe and B atoms in these two systems to be similar. Thus, a small negative spin polarization on the B atoms in $Nd_2Fe_{14}B$ is expected. The network structure in the spin-density map of $Nd_2Fe_{14}B$ (which is not the case for the FeB, Fe_2B, or the Fe_3B crystals) is therefore purely due to the rather unique structural configuration of the Fe atoms in the tetragonal $Nd_2Fe_{14}B$ crystal. The role of the rare-earth atoms is probably limited to providing the large crystal field and the resultant anisotropy in magnetization that is necessary for its exceptional permanent magnetic properties.[33]

VI. CONCLUSION

We have performed self-consistent spin-polarized electronic structure calculations on the ferromagnetic compounds FeB, Fe_2B, and Fe_3B using the OLCAO method. The results compare well with a large number of experimental measurements. It is shown that B 2s and 2p states are well below the Fermi level such that 0.5–0.6 electron is transferred from Fe to B. The bandwidth increases with the B concentration. The PDOS shows that the electronic structure in Fe-B compounds cannot be reduced to a simple model consisting of relatively isolated bands of Fe 4s, Fe 3d, B 2s, and B 2p. These orbitals are all hybridized in a subtle way depending on the local short-range order and the crystal symmetry. Also the Fe 3d bands, being more localized, are less affected. But even so, the exchange splitting depends on the B concentration, giving rise to different Fe moments in different crystals. The charge-density calculation shows a substantial degree of covalent bonding in Fe-B compounds and the spin-density map indicates that the B atoms are negatively polarized. The results of the present calculations also provide additional insight for the understanding of the electronic structure and magnetic properties of a-$Fe_{1-x}B_x$ glasses and $Nd_2Fe_{14}B$ permanent magnets.

ACKNOWLEDGMENTS

The work at the University of Missouri–Kansas City was supported by the U.S. Department of Energy (DOE) under the Grant No. De-FG02-84ER45170. The work at the Ames Laboratory was supported by the U.S. DOE under the Contract No. W-7405-Eng-82.

[1]P. J. Brown and J. L. Cox, Philos. Mag. **23**, 705 (1970).
[2]R. S. Perkins and P. J. Brown, J. Phys. F **4**, 906 (1974).
[3]D. J. Joyner, O. Johnson, D. M. Hercules, D. W. Bullett, and J. H. Weaver, Phys. Rev. B **24**, 3122 (1981); O. Johnson, D. J. Joyner, and D. M. Hercules, J. Phys. Chem. **84**, 542 (1980).
[4]G. Li and D. Wang, J. Phys. Cond. Matter **1**, 1799 (1989).
[5]Y. D. Zhang, J. I. Budnick, J. C. Ford, W. A. Hines, and F. H. Sanchez, J. Appl. Phys. **61**, 3231 (1987).
[6]R. Coehoorn, D. B. De Mooij, and C. De Waard, J. Magn. Magn. Mater. **80**, 101 (1989).
[7]T. Bjurstrom and H. Arnfelt, Z. Phys. Chem. B **4**, 469 (1929).
[8]F. Wever and A. Muller, Mitt. K. Wilhelm-Inst. Eisenforsch, Dusseldorf **11**, 193 (1930).
[9]R. W. G. Wyckoff, *Crystal Structures* (Interscience, New York, 1965), p. 114.
[10]B. N. Harmon, W. Weber, and D. R. Hamann, Phys. Rev. B **25**, 1109 (1982); W. Y. Ching and B. N. Harmon, *ibid.* **34**, 5305 (1986).
[11]W. Y. Ching, Y.-N. Xu, and K. W. Wong, Phys. Rev. B **40**, 8111 (1989).
[12]F. Zandiehnadem, R. A. Murray, and W. Y. Ching, Physica B+C **150B**, 19 (1988); Y.-N. Xu and W. Y. Ching, in *SiO_2 and Its Interfaces*, Vol. 99 of *Materials Research Society Symposium Proceedings*, edited by S. T. Pantelides and G. Lucovsky (MRS, Pittsburgh, 1988), p. 403; Phys. Rev. B **41**, 5471 (1990).
[13]P. J. Feibelman, J. A. Appelbaum, and D. R. Hamann, Phys. Rev. B **20**, 1433 (1979); J. A. Appelbaum and D. R. Hamann, in *Transition Metals*, edited by M. J. G. Lee, J. M. Perz, and E. Fawcett (Institute of Physics, Bristol, 1980), p. 111.
[14]Z.-Q. Gu and W. Y. Ching, Phys. Rev. B **33**, 2868 (1986); **36**, 8530 (1987).

[15]W. Y. Ching, Y.-N. Xu, G. L. Zhao, K. W. Wong, and F. Zandiehnadem, Phys. Rev. Lett. **59**, 1333 (1987); W. Y. Ching, G.-L. Zhao, Y.-N. Xu, and K. W. Wong, *Series on Progress in High Temperature Superconductivity,* edited by B. E. Baaquie, C. K. Chew, C. H. Lai, O. H. Oh, and K. K. Phua (World Scientific, Singapore, 1989), Vol. 12, p. 58.

[16]T. C. Leung, X. W. Wang, and B. N. Harmon, Phys. Rev. B **37**, 384 (1988).

[17]W. Y. Ching, L. W. Song, and S. S. Jaswal, Phys. Rev. B **30**, 544 (1984); W. Y. Ching, *ibid.* **34**, 2080 (1986); G.-L. Zhao and W. Y. Ching, Phys. Rev. Lett. **62**, 2511 (1989); W. Y. Ching, G. L. Zhao, and Yi He, Phys. Rev. B (to be published).

[18]X.-F. Zhong, Y.-N. Xu, and W. Y. Ching, Phys. Rev. B **41**, 10 545 (1990).

[19]J. F. Herbst, J. J. Croat, F. E. Pinkerton, and W. B. Yelon, Phys. Rev. B **29**, 4176 (1984).

[20]U. von Barth and L. Hedin, J. Phys. C **5**, 1629 (1972).

[21]V. L. Moruzzi, J. F. Janak, and A. R. Williams, *Created Electronic Properties of Metals* (Pergamon, New York, 1978).

[22]E. Clementi and C. Roetti, At. Data Nucl. Data Tables **14**, 177 (1974).

[23]A. Amamou and G. Krill, Solid State Commun. **33**, 1089 (1980).

[24]G. Bayreuther, G. Enders, H. Hoffman, U. Korndorfer, W. Oestreicher, K. Roll, and M. Takahashi, J. Magn. Magn. Mater. **31-34**, 1535 (1983).

[25]N. Cowlam and G. E. Carr, J. Phys. F **15**, 1109 (1985); **15**, 1117 (1985).

[26]Th. Paul and H. Neddermeyer, J. Phys. F **15**, 79 (1985).

[27]T. Fujiwara, J. Phys. F **12**, 661 (1982).

[28]R. Roy and A. K. Majumdar, Phys. Rev. B **31**, 2033 (1985).

[29]M. M. Abd-Elmeguid, H. Micklitz, and I. Vincze, Phys. Rev. B **25**, 1 (1982).

[30]W. Matz and H. Hermann, Phys. Status Solidi A **94**, 617 (1986).

[31]M. Matz, H. Hermann, and N. Mattern, J. Non-Cryst. Solids **93**, 217 (1987).

[32]F. H. Sanchez, J. I. Budnik, Y. D. Zhang, W. A. Hines, M. Choi, and R. Hasegawa, Phys. Rev. B **34**, 4738 (1986).

[33]X. F. Zhong and W. Y. Ching, Phys. Rev. B **39**, 12 018 (1989); **40**, 5292 (1989).